Journal of Magnetic Resonance 206 (2010) 112–119

Contents lists available at ScienceDirect

Journal of Magnetic Resonance

journal homepage: www.elsevier.com/locate/jmr

Double-wave-vector diffusion-weighting experiments with multiple concatenations at long mixing times

Marco Lawrenz, Jürgen Finsterbusch *

Department of Systems Neuroscience, University, Medical Center Hamburg-Eppendorf, Hamburg, Germany
Neuroimage Nord, University Medical Centers Hamburg-Kiel-Lübeck, Germany

ARTICLE INFO

Article history:
Received 20 November 2009
Revised 24 June 2010
Available online 30 June 2010

Keywords:
Double-wave-vector diffusion-weighting
Tensor model
Diffusion anisotropy
Microscopic anisotropy
MA
Multiple concatenations

ABSTRACT

MR sequences where two diffusion-weighting periods are applied successively in a single acquisition seem to be a promising tool for the investigation of tissue structure on a microscopic level such as the characterization of the compartment size or eccentricity measures of pores. However, the application of such double-wave-vector (DWV) experiments on whole-body MR systems is hampered by the long gradient pulses required that have been shown to reduce the signal modulation. In this work, it is demonstrated that involving multiple concatenations of the two diffusion-weighting periods can ameliorate this problem in experiments with long mixing times between the two wave vectors. The recently presented tensor equation is extended to multiple concatenations. As confirmed by Monte-Carlo simulations, this model shows a good approximation of the signals observed for typical whole-body gradient pulse durations and the derived anisotropy measures are obtained with good accuracy. Most importantly, the signal modulation is increased with multiple concatenations because shorter gradient pulses can be used to achieve the desired diffusion-weighting. Thus, the multiple concatenation approach may help to improve the applicability and reliability of DWV measurements with long mixing times on standard whole-body MR systems.

1. Introduction

In the past years, MR experiments involving two diffusion-weighting periods which are applied successively in the same acquisition have regained interest due to their sensitivity on tissue structure at the microscopic level [1–3]. Because for short gradient pulses a diffusion-weighting period is equivalent to a scatter event [4] which can be characterized by a wave vector, the term two- or double-wave-vector (DWV) diffusion-weighting has been used for such experiments in contrast to standard, single-wave-vector weighting [5]. Studies with DWV experiments at short mixing times between the two wave vectors have been used for the estimation of pore or compartment sizes [6–11].

In DWV experiments with long mixing times, the diffusion-weighted signal of cells with an isotropic orientation distribution is expected to differ between parallel and orthogonal wave vector orientations for anisotropic pores or cells [3]. This microscopic diffusion anisotropy effect that cannot be observed with standard single-wave-vector experiments has been demonstrated experimentally in a variety of samples [7,11–14], recently also on a whole-body MR system [15]. A tensor model based on the short-pulse approximation was proposed which describes the signal behavior in the fourth order of the wave vector amplitude q for arbitrary wave vectors, pores sizes and orientation distributions [16]. This approach can be used to derive rotationally invariant measures that characterize the microscopic diffusion anisotropy [16]. But signal equation calculations [17,18] as well as numerical simulations [19] performed for simple pore shapes and general timing parameters demonstrated that finite gradient pulse durations lead to a reduced modulation amplitude which is expected to hamper its detectability on whole-body MR systems.

In this work, multiple concatenations of the two wave vectors [20] with long mixing times are investigated for timing parameters compatible with whole-body MR systems. In the Theory part the recently developed tensor approach with its microscopic anisotropy measure *MA* [16] is extended to multiple concatenations. The extended theory and the respective numerical simulations are in good agreement for multiple concatenations for both, infinitesimal short as well as typical whole-body gradient pulse durations. For long gradient pulses, cell parameters and microscopic anisotropy measures derived from the simulations show some deviations. Most importantly, the signal modulation observed in experiments with multiple concatenations is increased because shorter gradient pulses can be used to achieve the desired diffusion-weighting. Thus, the detectability of the microscopic anisotropy effect in the DWV

* Corresponding author. Address: Institut für Systemische Neurowissenschaften, Geb. W34, Universitätsklinikum Hamburg-Eppendorf, Martinistrasse 52, 20246 Hamburg, Germany. Fax: +49 40 7410 59955.
E-mail address: j.finsterbusch@uke.uni-hamburg.de (J. Finsterbusch).

1090-7807/$ - see front matter © 2010 Elsevier Inc. All rights reserved.
doi:10.1016/j.jmr.2010.06.016

experiment at long mixing times could be improved, in particular, on whole-body MR systems.

2. Theory

In this section, the basic signal equations derived previously [16] are extended to multiple concatenations. Note that the derivation will not be fully reproduced here, the reader is referred to ref. [16] for a detailed synopsis. As for the simple DWV experiment, it is assumed, that for multiple concatenations of the two wave vectors (Fig. 1a) all pulse durations δ_i are short ($\delta_i \to 0$) and the diffusion times Δ_i are large compared to τ_D ($\Delta_i \gg \tau_D$) which is the time a spin typically needs to diffuse across a pore, i.e. $\tau_D = \frac{a^2}{2D}$ with the pore diameter a and the diffusion coefficient D. Furthermore, all pulse durations and diffusion times as well as all mixing times are set identical, i.e. $\delta_j = \delta$, $\Delta_j = \Delta$, and $\tau_{m,j} = \tau_m$.

2.1. Multiple concatenations at long mixing times

The NMR signal M for fully restricted diffusion in isolated pores or cells observed in a DWV diffusion-weighting experiment with wave vectors $\mathbf{q_1}$ and $\mathbf{q_2}$ was first evaluated by Mitra [3]. For the case that the mixing time τ_m between the two wave vectors is large compared to τ_D ($\tau_m \gg \tau_D$), he obtained

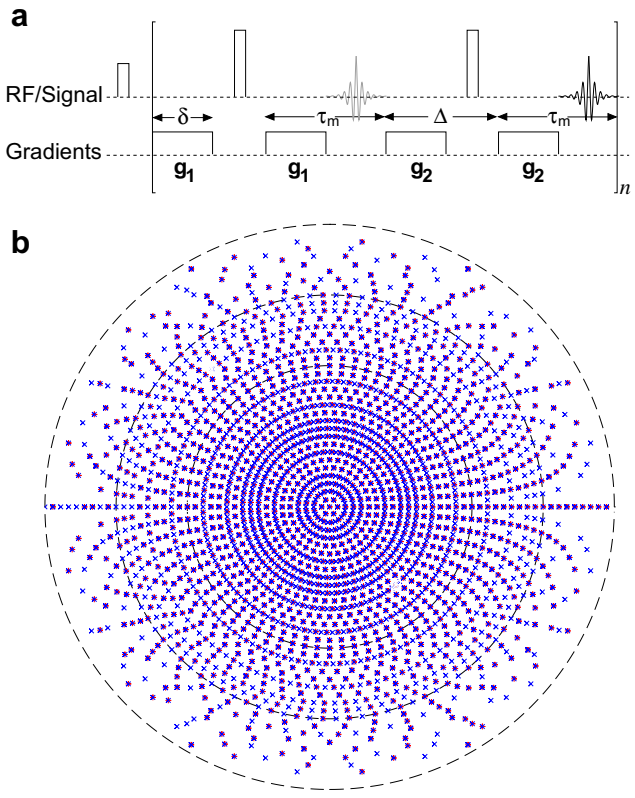

Fig. 1. (a) Example of a basic pulse sequence for a double-wave-vector (DWV) diffusion-weighting experiment with multiple concatenations of both wave vectors, i.e. each wave vector is applied n times. In the sequence shown, the two wave vectors alternate but it should be emphasized that the theoretical framework provided holds for any order and number of applications of the two diffusion-weighting periods. Note also that the important feature, two diffusion-weighting periods applied successively in a single experiment, can be realized with various pulse sequences and is not limited to the preparation shown here. (b) Polar plot of the wave vector directions used in the "isotropic" schema for the first (+, red) and second (×, blue) wave vector. The circles (black, dashed) represent azimuth angles of 90°, 180°, 270°, and 360° (from inner to outer). (For interpretation of the references to colour in this figure legend, the reader is referred to the web version of this article.)

$$M(\mathbf{q_1},\mathbf{q_2}) \propto \sum_{j=1}^{N} |\tilde{\rho}_j(\mathbf{q_1})|^2 |\tilde{\rho}_j(\mathbf{q_2})|^2 \tag{1}$$

where $\tilde{\rho}_j(\mathbf{q})$ is the Fourier transformation of the spin density distribution ρ_j in pore j

$$\tilde{\rho}_j(\mathbf{q}) = \int_{\text{pore}\,j} \rho_j(\mathbf{r}) e^{i\mathbf{qr}}\, d\mathbf{r}. \tag{2}$$

To simplify the following equations, the pore index is dropped.

For an ensemble of identical pores or cells with a single orientation under the application of multiple concatenations, the signal is given by [20]

$$M(n_1,n_2,\mathbf{q_1},\mathbf{q_2}) \propto |\tilde{\rho}(\mathbf{q_1})|^{2n_1} |\tilde{\rho}(\mathbf{q_2})|^{2n_2} \tag{3}$$

where n_1 and n_2 denote how often each wave vector appears. Note that Eq. (3) holds for any n_1 and n_2 and that it is independent of the order in which the individual wave vectors are applied [20]. However, in the presented simulations, only setups with alternating wave vectors (Fig. 1a) are considered.

2.2. Taylor expansion

Part of the expansion of Eq. (3) to fourth order has been shown previously [16] based on the expansion of $\tilde{\rho}$ to the same order: Using the rank-2 (3×3) tensor $\underline{\underline{\mathbf{R}}}$ and defining a rank-4 ($3 \times 3 \times 3 \times 3$) tensor $\underline{\underline{\mathbf{S}}}$ with elements

$$\begin{aligned} R_{jk} &= \int_{\text{pore}} \rho(\mathbf{r}) r_j r_k\, d\mathbf{r} \\ S_{jklm} &= \int_{\text{pore}} \rho(\mathbf{r}) r_j r_k r_l r_m\, d\mathbf{r}, \end{aligned} \tag{4}$$

$\tilde{\rho}$ can be re-written to

$$\begin{aligned} \tilde{\rho}(\mathbf{q}) = 1 &- \frac{1}{2}\mathbf{q}^T\underline{\underline{\mathbf{R}}}\mathbf{q} - \frac{i}{6}\sum_{j,k,l=1}^{3} q_j q_k q_l \int_{\text{pore}} \rho(\mathbf{r}) r_j r_k r_l\, d\mathbf{r} \\ &+ \frac{1}{24}\sum_{j,k,l,m=1}^{3} q_j q_k q_l q_m S_{jklm} + \mathcal{O}(q^5). \end{aligned} \tag{5}$$

This yields

$$\begin{aligned} \tilde{\rho}(\mathbf{q})^n = 1 &- \frac{n}{2}\mathbf{q}^T\underline{\underline{\mathbf{R}}}\mathbf{q} - \frac{in}{6}\sum_{j,k,l=1}^{3} q_j q_k q_l \int_{\text{pore}} \rho(\mathbf{r}) r_j r_k r_l\, d\mathbf{r} \\ &+ \frac{n(n-1)}{8}\left(\mathbf{q}^T\underline{\underline{\mathbf{R}}}\mathbf{q}\right)^2 + \frac{n}{24}\sum_{j,k,l,m=1}^{3} q_j q_k q_l q_m S_{jklm} + \mathcal{O}(q^5). \end{aligned} \tag{6}$$

Using these results, the Taylor expansion of $|\tilde{\rho}(\mathbf{q})|^{2n}$ can be calculated to

$$\begin{aligned} |\tilde{\rho}(\mathbf{q})|^{2n} &= \tilde{\rho}(\mathbf{q})^n \tilde{\rho}^*(\mathbf{q})^n \\ &= 1 - n\mathbf{q}^T\underline{\underline{\mathbf{R}}}\mathbf{q} + \frac{n^2}{4}(\mathbf{q}^T\underline{\underline{\mathbf{R}}}\mathbf{q})^2 + \frac{n}{12}\sum_{j,k,l,m=1}^{3} q_j q_k q_l q_m S_{jklm} \\ &\quad + \frac{n(n-1)}{4}(\mathbf{q}^T\underline{\underline{\mathbf{R}}}\mathbf{q})^2 + \mathcal{O}(q^6). \end{aligned} \tag{7}$$

Note that the imaginary third order term of Eq. (5) only contributes to sixth order terms which are neglected here.

Thus, the expansion of Eq. (3) up to fourth order yields

$$\begin{aligned} M(n_1,n_2,\mathbf{q_1},\mathbf{q_2}) \propto 1 &- \sum_{v=1}^{2} n_v \mathbf{q_v}^T\underline{\underline{\mathbf{R}}}\mathbf{q_v} + \frac{1}{4}\sum_{v=1}^{2}(2n_v-1)n_v(\mathbf{q_v}^T\underline{\underline{\mathbf{R}}}\mathbf{q_v})^2 \\ &+ n_1 n_2\left(\mathbf{q_1}^T\underline{\underline{\mathbf{R}}}\mathbf{q_1}\right)(\mathbf{q_2}^T\underline{\underline{\mathbf{R}}}\mathbf{q_2}) \\ &+ \frac{1}{12}\sum_{v=1}^{2}\sum_{j,k,l,m=1}^{3} n_v q_{v,j} q_{v,k} q_{v,l} q_{v,m} S_{jklm} + \mathcal{O}(q^6) \end{aligned} \tag{8}$$

where $\mathbf{q}_{v,j}$ represents the jth component of wave vector $\mathbf{q}_v$. It should be kept in mind that $\tau_m \gg \tau_D$ is assumed for the derivation of Eq. (8).

Although Eq. (8) is already the desired general signal equation for multiple concatenations, a different notation is used which allows for a more convenient treatment of the fourth order terms.

2.3. Modified Voigt notation

The modified Voigt notation [21] can be applied for a further simplification of Eq. (8). With the help of a six element vector $\tilde{\mathbf{q}}$ with

$$\tilde{\mathbf{q}} = \left(q_1^2, q_2^2, q_3^2, q_1q_2, q_1q_3, q_2q_3\right)^T \tag{9}$$

for each wave vector $\mathbf{q}_v$ and defining the matrices

$$\underline{\underline{\tilde{\mathbf{S}}}} = \begin{pmatrix} S_{1111} & S_{1122} & S_{1133} & 2S_{1112} & 2S_{1113} & 2S_{1123} \\ S_{1122} & S_{2222} & S_{2233} & 2S_{1222} & 2S_{1223} & 2S_{2223} \\ S_{1133} & S_{2233} & S_{3333} & 2S_{1233} & 2S_{1333} & 2S_{2333} \\ 2S_{1112} & 2S_{1222} & 2S_{1233} & 4S_{1122} & 4S_{1123} & 4S_{1223} \\ 2S_{1113} & 2S_{1223} & 2S_{1333} & 4S_{1123} & 4S_{1133} & 4S_{1233} \\ 2S_{1123} & 2S_{2223} & 2S_{2333} & 4S_{1223} & 4S_{1233} & 4S_{2233} \end{pmatrix} \tag{10}$$

and

$$\underline{\underline{\tilde{\mathbf{R}}}} = \begin{pmatrix} R_{11}^2 & R_{11}R_{22} & R_{11}R_{33} & 2R_{11}R_{12} & 2R_{11}R_{13} & 2R_{11}R_{23} \\ R_{11}R_{22} & R_{22}^2 & R_{22}R_{33} & 2R_{12}R_{22} & 2R_{13}R_{22} & 2R_{22}R_{23} \\ R_{11}R_{33} & R_{22}R_{33} & R_{33}^2 & 2R_{12}R_{33} & 2R_{13}R_{33} & 2R_{23}R_{33} \\ 2R_{11}R_{12} & 2R_{12}R_{22} & 2R_{12}R_{33} & 4R_{12}^2 & 4R_{12}R_{13} & 4R_{12}R_{23} \\ 2R_{11}R_{13} & 2R_{13}R_{22} & 2R_{13}R_{33} & 4R_{12}R_{13} & 4R_{13}^2 & 4R_{13}R_{23} \\ 2R_{11}R_{23} & 2R_{22}R_{23} & 2R_{23}R_{33} & 4R_{12}R_{23} & 4R_{13}R_{23} & 4R_{23}^2 \end{pmatrix}, \tag{11}$$

the terms of Eq. (8) can be re-written to

$$M(n_1, n_2, \mathbf{q_1}, \mathbf{q_2}) \propto 1 - \sum_{v=1}^{2} n_v \mathbf{q}_v^T \underline{\underline{\mathbf{R}}} \mathbf{q}_v + \sum_{v=1}^{2} \frac{n_v}{4}(2n_v - 1)\tilde{\mathbf{q}}_v^T \underline{\underline{\tilde{\mathbf{R}}}} \tilde{\mathbf{q}}_v + n_1 n_2 \tilde{\mathbf{q}}_1^T \underline{\underline{\tilde{\mathbf{R}}}} \tilde{\mathbf{q}}_2 + \frac{1}{12} \sum_{v=1}^{2} n_v \tilde{\mathbf{q}}_v^T \underline{\underline{\tilde{\mathbf{S}}}} \tilde{\mathbf{q}}_v. \tag{12}$$

2.4. Tensor equation

With a conjunction of the four vectors $\mathbf{q}_v$ and $\tilde{\mathbf{q}}_v$ to two vectors $\mathbf{Q} = (\mathbf{q}_1^T, \mathbf{q}_2^T)^T$ and $\tilde{\mathbf{Q}} = (\tilde{\mathbf{q}}_1^T, \tilde{\mathbf{q}}_2^T)^T$, respectively, and utilizing the identity

$$n_1 n_2 \tilde{\mathbf{q}}_1^T \underline{\underline{\tilde{\mathbf{R}}}} \tilde{\mathbf{q}}_2 = n_1 n_2 \tilde{\mathbf{q}}_2^T \underline{\underline{\tilde{\mathbf{R}}}} \tilde{\mathbf{q}}_1 = \frac{n_1 n_2}{2}\left(\tilde{\mathbf{q}}_1^T \underline{\underline{\tilde{\mathbf{R}}}} \tilde{\mathbf{q}}_2 + \tilde{\mathbf{q}}_2^T \underline{\underline{\tilde{\mathbf{R}}}} \tilde{\mathbf{q}}_1\right) \tag{13}$$

the final tensor equation

$$M(n_1, n_2, \mathbf{Q}) \propto 1 - \frac{1}{2}\mathbf{Q}^T \underline{\underline{\mathbf{T}_\mathbf{a}}}(n_1, n_2)\mathbf{Q} + \frac{1}{12}\tilde{\mathbf{Q}}^T \underline{\underline{\tilde{\mathbf{U}}}}(n_1, n_2)\tilde{\mathbf{Q}} \tag{14}$$

is obtained where the symmetric second order (6×6) tensor

$$\underline{\underline{\mathbf{T}_\mathbf{a}}}(n_1, n_2) = \begin{pmatrix} 2n_1 \underline{\underline{\mathbf{R}}} & 0 \\ 0 & 2n_2 \underline{\underline{\mathbf{R}}} \end{pmatrix} \tag{15}$$

and the symmetric fourth order (12×12) tensor

$$\underline{\underline{\tilde{\mathbf{U}}}}(n_1, n_2) = \begin{pmatrix} n_1 \underline{\underline{\tilde{\mathbf{S}}}} + (3n_1(2n_1 - 1))\underline{\underline{\tilde{\mathbf{R}}}} & 6n_1 n_2 \underline{\underline{\tilde{\mathbf{R}}}} \\ 6n_1 n_2 \underline{\underline{\tilde{\mathbf{R}}}} & n_2 \underline{\underline{\tilde{\mathbf{S}}}} + (3n_2(2n_2 - 1))\underline{\underline{\tilde{\mathbf{R}}}} \end{pmatrix}, \tag{16}$$

respectively, are included. For $n_1 = n_2 = n$, the tensor $\underline{\underline{\tilde{\mathbf{U}}}}(n_1, n_2)$ can be simplified to

$$\underline{\underline{\tilde{\mathbf{U}}}}(n) = \begin{pmatrix} n\underline{\underline{\tilde{\mathbf{S}}}} + (3n(2n - 1))\underline{\underline{\tilde{\mathbf{R}}}} & 6n^2 \underline{\underline{\tilde{\mathbf{R}}}} \\ 6n^2 \underline{\underline{\tilde{\mathbf{R}}}} & n\underline{\underline{\tilde{\mathbf{S}}}} + (3n(2n - 1))\underline{\underline{\tilde{\mathbf{R}}}} \end{pmatrix}. \tag{17}$$

With Eq. (14), a general expression for the MR signal in a DWV experiment with multiple concatenations at long mixing times has been derived under the assumptions $\tau_m, \Delta \gg \tau_D$ and $\delta \to 0$. This equation conveniently describes the desired generalized signal for any wave vector direction and cell shape. For a mixture of different pore ensembles, the equation remains valid if the weighted sums of the individual ensembles are used as described previously [16].

2.5. Rotational invariant measures I_{MA} and MA and isotropic orientation distribution

It has been shown that the measures I_{MA} and MA according to

$$I_{MA} = \sum_{k=1}^{3} \tilde{R}_{kk} - \sum_{\substack{k,l=1 \\ k<l}}^{3} \tilde{R}_{kl} + \frac{3}{4}\sum_{m=4}^{6} \tilde{R}_{mm}$$
$$MA = \sqrt{\sum_{k=1}^{3} \tilde{R}_{kk} - \sum_{\substack{k,l=1 \\ k<l}}^{3} \tilde{R}_{kl} + \frac{3}{4}\sum_{m=4}^{6} \tilde{R}_{mm}} \Big/ \sum_{k=1}^{3} R_{kk} \tag{18}$$

are rotational invariants and reflect the diffusion anisotropy at the microscopic level [16]. For multiple concatenations, n_1 and n_2 need to be considered in the calculation of I_{MA} on the basis of 15 measured signals according to

$$I_{MA} = \frac{1}{n_1 n_2}\left(\sum_{k=1}^{3} M_{k,k} - \sum_{\substack{k,l=1 \\ k<l}}^{3} M_{k,l} + \frac{3}{2}\sum_{\substack{k,l=1 \\ k<l}}^{3}\left(\frac{1}{2}M_{kl,kl} + \frac{1}{2}M_{k\bar{l},k\bar{l}} - M_{kl,k\bar{l}}\right)\right). \tag{19}$$

Here, $M_{k,l}$ is the signal obtained for the two wave vectors along the axes $\mathbf{e_k}$ and $\mathbf{e_l}$, $M_{ij,kl}$ that one obtained for the two wave vectors along the diagonals $\mathbf{e_i} + \mathbf{e_j}$ and $\mathbf{e_k} + \mathbf{e_l}$. $k\bar{l}$ describes the diagonal $\mathbf{e_k} - \mathbf{e_l}$. Thus, Eq. (19) demonstrates that 15 measurements (or simulations) with different wave vector direction combinations are required to determine I_{MA} and the microscopic anisotropy MA [16].

Furthermore, the special case of a pore ensemble with an isotropic orientation distribution of identical cells is considered. The calculation given in the Appendix is straightforward and follows the way presented earlier [16]. Most notably, the signal damping in the second order depends linearly on n and the amplitude of the modulation is proportional to $n^2(\langle R_{kk}^2\rangle - \langle R_{kk}R_{ll}\rangle)$, i.e. to the square of n MA (see Appendix).

3. Experimental

Monte-Carlo simulations were performed to establish the derived tensor equation for multiple concatenations. The self-written IDL algorithm (version 7.0, ITT Visual Information Solutions, Boulder, USA) described previously [22] was extended to account for multiple concatenations. Starting for each spin with a random position within the pore volume, the spins performed a random, Gaussian displacement in a random direction in every time unit dt = 10 μs. At the pore boundaries, diffuse reflection was assumed. Identical wave vector amplitudes were used for both wave vectors ($|\mathbf{q}_v| = q$) in each simulation, possible relaxation effects were neglected. For every simulation a pool of 10,000 spins was investigated. As pore population, parallel oriented and isotropically distributed spheroidal pores with radii of 1.5 μm, 1.5 μm, and 5.0 μm were used. Relaxation effects were neglected.

Three different direction schemes were used for the orientations of the two wave vectors to investigate different aspects of the theoretical considerations: (i) the "isotropic" schema, (ii) the "tensor" schema and (iii) the "anisotropy" schema (compare ref.

[16]). In the isotropic schema, the directions of both wave vectors (1651 for the first and 3302 for the second wave vector) were uniformly distributed over a sphere (Fig. 1b). Those for the first wave vector were obtained by considering 36 circles of latitude in steps of 5°. On each circle, equidistant directions were defined with a number of directions proportional to the circle's circumference with a maximum number of 72 on the equator (corresponding to a seperation of 5°) yielding the 1651 directions for the first wave vector. By including the antipode for each of these directions, the 3302 directions for the second wave vector were obtained. In the simulations, each direction combination of the two wave vectors was investigated, i.e. a total number of $1651 \times 3302 \approx 5.45$ million different combinations was considered. The simulation results can then either be fitted to Eq. (14) to obtain the 42 tensor elements if all direction combinations are considered individually or to Eq. (A.8) to estimate the microscopic anisotropy if an isotropic orientation distribution is mimicked by averaging all wave vector combinations enclosing the same angle θ [16].

The tensor and anisotropy direction schemes were derived from nine directions covering the three directions along the coordinate axes, $(100)^T$, $(010)^T$, and $(001)^T$, and the six planar diagonals $(110)^T$, $(1-10)^T$, $(101)^T$, $(10-1)^T$, $(011)^T$, and $(01-1)^T$. The tensor scheme consisted of all 45 order-indendent combinations of these nine directions and is expected to be sufficient to derive the full tensor information, i.e. all 42 independent tensor elements [16]. The anisotropy scheme is a subset of 15 combinations originating from the tensor scheme and represents the minimum number of combinations from which the microscopic anisotropy information can be derived. It can be calculated according to Eq. (19) [16], i.e. the 15 different signal terms appearing in this equation define the 15 direction combinations used in the anisotropy scheme. All data were fitted with a Levenberg–Marquardt algorithm.

All mixing times τ_{mj} and all diffusion times Δ_j were set to an equal length of 30 ms. For the diffusion coefficient 2.0×10^{-3} mm^2 s^{-1} was used. One to six concatenations in maximum were used (see Fig. 1a). When comparing simulations with a different number of concatenations, the product nq^2, i.e. the diffusion-weighting, was kept constant to obtain a comparable signal decay.

In the first step, the validity of the extended tensor approach to describe the MR signal in experiments with multiple concatenations was confirmed. Therefore, the three schemes were applied to the pore species (single pore orientation) under a variation of the number of concatenations n for the shortest gradient pulse duration possible (10 μs). In the second step, the effect of finite pulses was studied using gradient amplitudes achievable on whole-body MR systems. Again, a constant nq^2 was used when varying the number of concatenations n and realized by using the same gradient amplitude but shortening δ according to $\delta \propto \frac{1}{\sqrt{n}}$ yielding pulse durations between 24 ms for $n = 1$ and 9.8 ms for $n = 6$ concatenations. To study the detectability of the presented approach in vivo, different gradient amplitudes achievable with standard whole-body gradient coils (39 mT/m), cutting-edge whole-body gradient systems (60 mT/m) [23,24], and a head gradient insert (78 mT/m) [25] were used in the simulations.

The deviations of the pore-size parameters or tensor elements that were determined from the fits, i.e. from their nominal values that can be calculated analytically, are given as a percentage. For those parameters or elements that have a nominal value of zero, the percentage is given relative to the non-vanishing nominal parameter or element with the lowest absolute value.

4. Results

In Fig. 2, the simulation results for the ideal case of infinitesimal short gradient durations are shown for the three wave vector schemas used. For a single pore species of parallel ellipsoidal cells, the

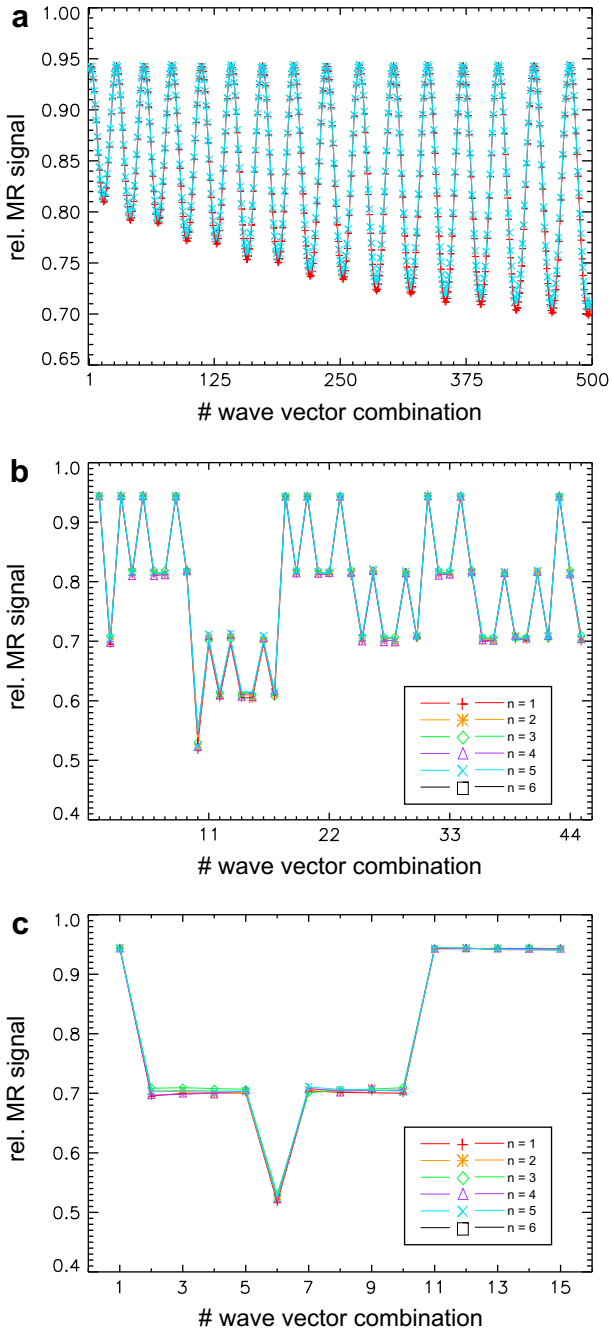

Fig. 2. Simulated MR signals (symbols) and fits to the tensor equation (lines) obtained for short (10 μs) gradient pulses and parallel oriented ellipsoidal pores with semi-axes of 1.5, 1.5, and 5.0 μm with (a) the isotropic, (b) the tensor and (c) the anisotropy direction scheme. In all plots, the x-axis represents the index of the wave vector orientation combination. In (a), only a subset covering 500 wave vector combinations (x-axis) is plotted where each data point represents the signal obtained for a certain combination of the wave vector orientations. The two data sets shown were simulated for $n = 1$ (+, red) and $n = 5$ (×, blue). The solid lines represent the fit of all (more than 5.45 million) combinations to Eq. (14). In (b) and (c) the MR signal covering 45 and 15 wave vector combinations (x-axis) was simulated with n varied from one to five. For all simulations a fixed nq^2 of 0.06 m^{-2} was used. Note that all plots cover not only different absolute wave vector orientations but also different relative angles between the two wave vetors. For details see text. (For interpretation of the references to colour in this figure legend, the reader is referred to the web version of this article.)

MR signal curves show pronounced modulations with the wave vector combination applied. Some minor signal deviation between the different numbers of concatenations below 1% can be noticed that similarly has been found earlier [16,22]. This may be caused

by an influence of a not sufficiently long mixing time, by rounding errors, or the hidden algorithm of the random number generator.

In Fig. 2a, a subset of the simulated MR data for the same pore species is shown which was obtained with the isotropic direction scheme. Each MR signal observed for a certain orientation combination of the two wave vectors relative to the orientation of the ellipsoidal pore is represented by one data point. Although only a small range of the over 5.4 million data points is shown, the fits to Eq. (14) based on all data approximate the simulation very well; the underlying pore-size parameters are in a good agreement with the nominal values with a maximum deviation of about 5% for all concatenations. This demonstrates the feasibility of the extended tensor equation to describe the signal for arbitrary pore and wave vector orientations accurately even in the general case of multiple concatenations.

Because the signal behavior described by Eq. (14) requires 42 different parameters in general, the tensor direction scheme containing 45 wave vector orientation combinations can be efficiently used for a determination of all parameters describing the signal behavior (see ref. [16] for details). Simulation results for the tensor scheme on the ellipsoidal cells with a single pore orientation along the *x*-axis are shown in Fig. 2b supplemented with the fits to the tensor equation. The signal amplitudes accumulate at a few different "levels" similar to the case without concatenations. Although some deviations of the data are visible, the fits to the general tensor equation for the different concatenations are in good agreement with the simulated data and yield pore parameters that differ by less than 1% between the different pore orientations and are within 5% of the nominal values.

Fig. 2c shows the simulations obtained with the anisotropy direction scheme. Here, the deviations are also minor and the fit to the tensor equation yields the same results in the limits of the accuracy as described before. Thus, the extended formalism including multiple concatenations has the potential to describe the signal reliably from a reasonable and realizable number of wave vector orientation combinations.

For the second step, the simulations were repeated for the gradient amplitudes achievable with whole-body MR systems. The signal curves obtained with the longer pulse lengths look very similar but there are important differences compared to Fig. 2: The signal decay as well as the modulation amplitude are considerably reduced. For the standard experiment ($n = 1$) the maximum modulation amplitude for the subset of the isotropic schema shown is reduced by a factor of about four, for the longer pulses from 0.25 (Fig. 2a) to 0.06 (Fig. 3a). A similar decrease is observed for the other direction schemas. As a consequence, the pore-size parameters derived from the fits are underestimated by up to 80%. The anisotropy measure *MA* obtained deviates from the nominal value by only about 25%.

With an increasing number of concatenations, a pronounced increase of the signal modulation is visible for all direction schemas, e.g. almost doubled to 0.12 for six concatenations in Fig. 3a. This not only improves the detectability of the signal modulation but also yields more accurate pore-size parameters that deviate by less than 50% from the nominal values (Fig. 3b). Similarly, the anisotropy measure *MA* can be determined with an accuracy of about 10% ($n = 6$, Fig. 3c).

Considering an isotropic distribution of the pores (Fig. 4) the signals show more deviation from the fits, in particular around parallel and anti-parallel wave vector orientations. Most likely, this is due to a remaining undersampling of the corresponding angles, i.e. the distribution of the wave vector combinations with these angles is not perfectly isotropic. Nevertheless, the deviation from the fit was found to be negligibly small (below 0.5%). As in Fig. 3, multiple concatenations improve the signal modulation amplitude, e.g. by a factor of about three for $n = 6$ compared to the standard experiment. However, as can be seen in Fig. 3a, the absolute signal difference between a parallel and an orthogonal combination of the two wave

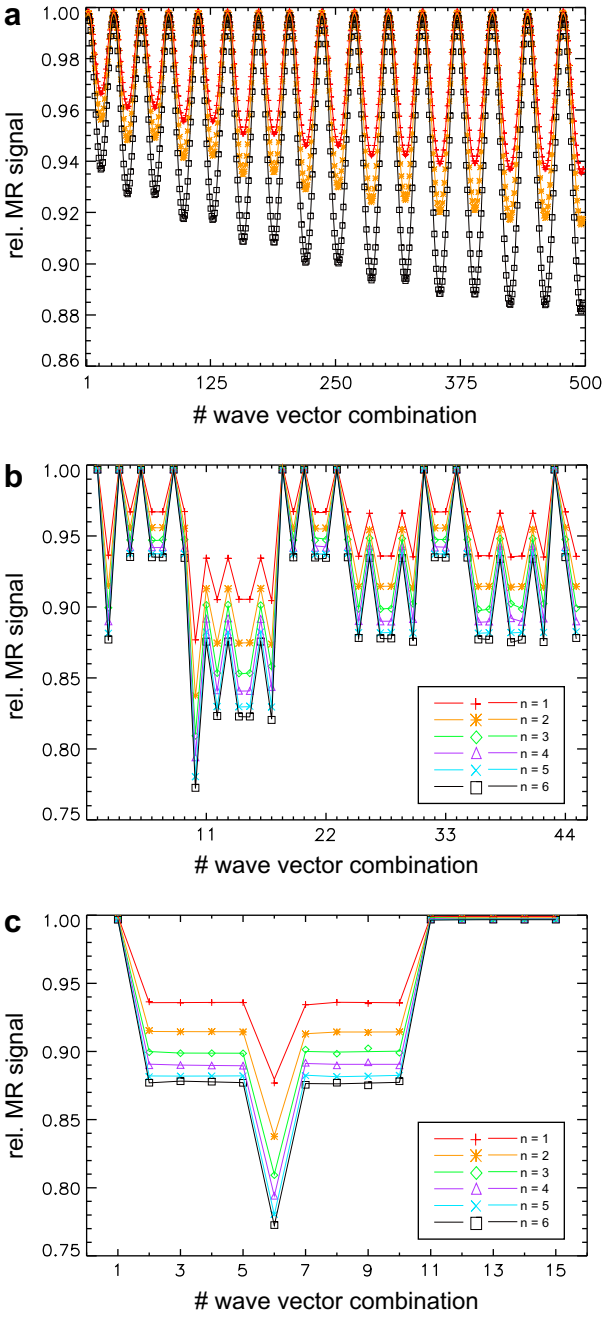

Fig. 3. Simulated MR signals (symbols) and fits to the tensor equation (lines) obtained for gradient pulse durations and gradient amplitudes (39 mT/m) achievable with whole-body MR systems. nq^2 was fixed (0.06 m^{-2}) yielding gradient pulse durations δ between 24 ms ($n = 1$) and 9.8 ms ($n = 6$). The number of concatenations equals $n = 1$, 2 and 6 in Fig. 3a and one to six in (b) and (c), respectively. All data sets show an increase of the signal modulation amplitude with increasing number of concatenations (top to bottom). In all plots, the *x*-axis represents the index of the wave vector orientation combination. Note that all plots cover not only different absolute wave vector orientations but also different relative angles between the two wave vetors.

vectors is small and may be difficult to detect on standard whole-body MR systems even for six concatenations. Some improvement could be achieved with a higher gradient amplitude (Fig. 4b) that can be realized by using more than one physical gradient axis. For instance, using the wave vector directions $(1\,1\,0)^T$ and $(1\,-1\,0)^T$ still allows to measure parallel and orthogonal orientations but increases the effective gradient amplitude by a factor of $\sqrt{2}$. A further improvement is observed for 78 mT/m with a signal modulation of 1.9% for two concatenations and 3.9% for six concatenations. Such

experiments could be performed with cutting-edge whole-body gradient systems (60 mT/m) [23,24] using the more efficient wave directions mentioned above or with dedicated gradient inserts available from some manufactures, e.g. compare ref. [25].

5. Discussion

The extension of the double-wave-vector diffusion-weighting experiment with long mixing times to multiple concatenations of the two diffusion-weighting periods was presented. The tensor approach derived previously for the simple experiment [16] has been extended accordingly yielding an equation that describes the signal amplitude depending on the two wave vectors not only for arbitrary cell or pore shapes and orientation distributions but also for any number of concatenations. In the first part, it has been demonstrated with numerical simulations of diffusion in ellipsoidal pores that the derived equation yields a good fit and accurate estimates of the pore parameters for short gradient pulses. In the second step it could be shown, that the model fits the simulations performed very well also for gradient pulse amplitudes and durations compatible with whole-body MR systems. Thereby, the signal modulation amplitude is considerably reduced, in particular for the simple experiments yielding pore-size parameters reduced by a factor of up to five and *MA* values reduced by 25%. However, with multiple concatenations the pore parameters can be obtained with an improved accuracy, i.e. about 50% and only 10% deviation for the pore-size parameters and the *MA*, respectively.

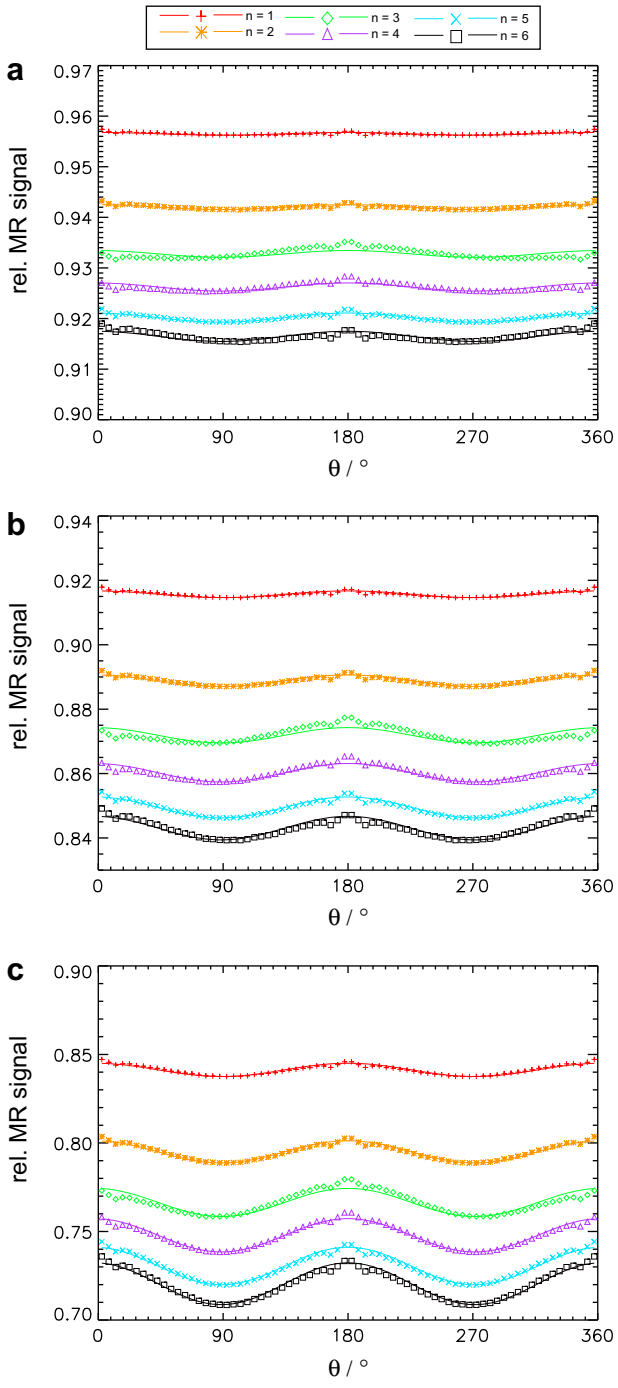

Fig. 4. Simulated MR signals (symbols) for an isotropic orientation distribution of the ellipsoidal pores (semi-axes 1.5, 1.5, and 5 μm) vs. the angle θ between the two wave vectors. One to six concatenations (see legend) were used, the lines represent the fits to Eq. (A.8). A fixed nq^2 was used in each subfigure yielding pulse durations between 24.0 ms ($n = 1$) and 9.8 ms ($n = 6$). Gradient amplitudes were varied between (a) 39 mT/m, (b) 55 mT/m, and (c) 78 mT/m, i.e. nq^2 equals 0.06 m^{-2}, 0.12 m^{-2}, and 0.24 m^{-2}, respectively.

The observed underestimation of the pore-size parameters for pulse durations compatible with whole-body MR systems is caused by the violation of the short-pulse approximation underlying the theoretical considerations. It is consistent with initial results obtained with a multiple propagator approach introduced to calculate the effect of finite pulse durations in ellipsoidal pores for the simple DWV experiment [26]. Analogously, in numerical simulations performed to investigate the anisotropy effect, a decrease of the signal difference between parallel and orthogonal wave vector orientations for long pulse durations has been reported, e.g. by about 16% for 20 ms-pulses and larger pores (semi-axes 2.5, 2.5, and 7.5 μm) [19]. A similar phenomenon was also observed for the compartment size estimation with simple DWV experiments employing a short mixing time τ_m [19]. Because the size estimates were in good agreement with the real values for the short (10 μs) gradient pulses, the effect of the finite diffusion and mixing time (both 30 ms) seems to be marginal in the present simulations.

Compared to the pore-size parameters, the estimates *MA* are much more reasonable, e.g. with an error of about 10% for a simulation where the pore sizes are underestimated by about 50%. This is a consequence of the fact that a systematic underestimation is present in all directions, i.e. along the short axis as well as along the long axis of the ellipsoids. Thus, the *MA* of the (under)estimated pore is similar to that of the real pore. However, the deviation depends on the pore size along the measured directions which introduces a slight distorsion of the *MA* for the ellipsoidal pores investigated.

It should be emphasized that the prolonged echo time, or more general the longer sequence timing, for multiple concatenations is accompagnied by increased relaxation-induced signal losses. Thus, the improved relative signal modulation reported for multiple concatenations will not convert to an equivalently higher absolute signal modulation. In particular for a large number of concatenations, the absolute modulation may even decrease. The trade-off between the reduced signal-to-noise and the increased relative signal modulation is expected to depend not only on the sample's relaxation times but also on the pore sizes present.

Despite the pronounced improvement for multiple concatenations at the long gradient pulse durations required on whole-body MR systems, the signal modulation amplitude may still be quite small as has been demonstrated for an isotropic orientation distribution. Thus, to improve the detectability more efficient direction schemes may be required that use several physical gradient axes simultaneously. A further enhancement of the modulation is expected for stronger gradient systems that are becoming more and more available for whole-body MR systems, or head gradient inserts [23–25]. Both would allow to apply long mixing time DWV experiments to human white matter in vivo which would be a

particularly interesting target because an estimation of the microscopic anisotropy may help to distinguish between fiber density and fiber coherence in regions with low macroscopic diffusion anisotropy. In this context, it should also be mentioned that a higher signal modulation may be expected for white matter fibers as their pore-shape related anisotropy is more pronounced than in the ellipsoidal pores investigated here.

6. Conclusions

The tensor model of double-wave-vector experiments with long mixing times has been extended to multiple concatenations of the two diffusion weighting periods and confirmed by numerical simulations. The diffusion-weighting per wave vector can be reduced for multiple concatenations which reduces the pulse durations that are known to have an adverse effect on the signal modulation. Thus, not only the detectability is improved by also the accuracy of the pore-parameters derived in particular on whole-body MR systems.

Acknowledgment

This work was supported by the Bundesministerium für Bildung und Forschung (Neuroimage Nord).

Appendix A

The tensors $\underline{\underline{\mathbf{R}}}$ and $\underline{\underline{\mathbf{S}}}$ derived depend on the pore orientation Ψ. To consider an isotropic orientation distribution an average over all possible pore orientation needs to be performed yielding the effective tensors $\underline{\underline{\mathbf{R}}}_{\mathbf{iso}}$ and $\underline{\underline{\mathbf{S}}}_{\mathbf{iso}}$ which are given by [16]

$$\underline{\underline{\widetilde{\mathbf{R}}}}_{\mathbf{iso}} = \frac{1}{15}\begin{pmatrix} \langle R_{kk}^2\rangle & \langle R_{kk}R_{ll}\rangle & \langle R_{kk}R_{ll}\rangle & 0 & 0 & 0 \\ \langle R_{kk}R_{ll}\rangle & \langle R_{kk}^2\rangle & \langle R_{kk}R_{ll}\rangle & 0 & 0 & 0 \\ \langle R_{kk}R_{ll}\rangle & \langle R_{kk}R_{ll}\rangle & \langle R_{kk}^2\rangle & 0 & 0 & 0 \\ 0 & 0 & 0 & 4\langle R_{kl}^2\rangle & 0 & 0 \\ 0 & 0 & 0 & 0 & 4\langle R_{kl}^2\rangle & 0 \\ 0 & 0 & 0 & 0 & 0 & 4\langle R_{kl}^2\rangle \end{pmatrix} \tag{A.1}$$

with

$$\begin{aligned} \langle R_{kk}^2\rangle &= \int_{\Psi} R_{\Psi',11}^2 d\Psi' = 3\sum_k R_{kk}^2 + 2\sum_{\substack{k,l \\ k<l}} R_{kk}R_{ll} \\ \langle R_{kk}R_{ll}\rangle &= \int_{\Psi} R_{\Psi',11}R_{\Psi',22} d\Psi' = \sum_k R_{kk}^2 + 4\sum_{\substack{k,l \\ k<l}} R_{kk}R_{ll} \\ \langle R_{kl}^2\rangle &= \int_{\Psi} R_{\Psi',12}^2 d\Psi' = \sum_k R_{kk}^2 - \sum_{\substack{k,l \\ k<l}} R_{kk}R_{ll}, \end{aligned} \tag{A.2}$$

where $\underline{\underline{\mathbf{R}}}'_{\Psi}$ represents the tensor $\underline{\underline{\mathbf{R}}}$ for the pore orientation Ψ' and

$$\underline{\underline{\widetilde{\mathbf{S}}}}_{\mathbf{iso}} = \frac{1}{15}\begin{pmatrix} \langle S_{kkkk}\rangle & \langle S_{kkll}\rangle & \langle S_{kkll}\rangle & 0 & 0 & 0 \\ \langle S_{kkll}\rangle & \langle S_{kkkk}\rangle & \langle S_{kkll}\rangle & 0 & 0 & 0 \\ \langle S_{kkll}\rangle & \langle S_{kkll}\rangle & \langle S_{kkkk}\rangle & 0 & 0 & 0 \\ 0 & 0 & 0 & 4\langle S_{kkll}\rangle & 0 & 0 \\ 0 & 0 & 0 & 0 & 4\langle S_{kkll}\rangle & 0 \\ 0 & 0 & 0 & 0 & 0 & 4\langle S_{kkll}\rangle \end{pmatrix} \tag{A.3}$$

with $\langle S_{kkkk}\rangle = 3\langle R^4\rangle$, $\langle R^4\rangle = \int r^4 d\mathbf{r}$, and $\langle S_{kkll}\rangle = \langle R^4\rangle$. The signal contribution related to $\underline{\underline{\mathbf{R}}}_{\mathbf{iso}}$ in Eq. (14) yields

$$\begin{aligned} &\widetilde{\mathbf{Q}}^T \begin{pmatrix} 3(2n_1-1)n_1\underline{\underline{\widetilde{\mathbf{R}}}}_{iso} & 6n_1n_2\underline{\underline{\widetilde{\mathbf{R}}}}_{\mathbf{iso}} \\ 6n_1n_2\underline{\underline{\widetilde{\mathbf{R}}}}_{\mathbf{iso}} & 3(2n_2-1)n_2\underline{\underline{\widetilde{\mathbf{R}}}}_{iso} \end{pmatrix} \\ &\widetilde{\mathbf{Q}} = \frac{1}{5}\langle R_{kk}R_{ll}\rangle q^4\left(2\left(n_1^2+n_2^2\right)+4n_1n_2-(n_1+n_2)\right) \\ &\quad + \frac{2}{5}\langle R_{kl}^2\rangle q^4\left(2\left(n_1^2+n_2^2\right)+2n_1n_2-(n_1+n_2)+2n_1n_2\cos 2\theta\right). \end{aligned} \tag{A.4}$$

In the case $n_1 = n_2 = n$, Eq. (A.4) reduces to

$$\begin{aligned} &\widetilde{\mathbf{Q}}^T \begin{pmatrix} 3(2n-1)n\underline{\underline{\widetilde{\mathbf{R}}}}_{\mathbf{iso}} & 6n^2\underline{\underline{\widetilde{\mathbf{R}}}}_{\mathbf{iso}} \\ 6n^2\underline{\underline{\widetilde{\mathbf{R}}}}_{\mathbf{iso}} & 3(2n-1)n\underline{\underline{\widetilde{\mathbf{R}}}}_{iso} \end{pmatrix} \\ &\widetilde{\mathbf{Q}} = \frac{1}{5}\langle R_{kk}R_{ll}\rangle q^4(8n^2-2n) + \frac{2}{5}\langle R_{kl}^2\rangle q^4((6n^2-2n)+2n^2\cos 2\theta). \end{aligned} \tag{A.5}$$

Thus, a dependency of the signal on the angle θ between the two wave vectors is obtained. The fourth order signal contribution related to $\underline{\underline{\widetilde{\mathbf{S}}}}_{\mathbf{iso}}$ can be written as

$$\widetilde{\mathbf{Q}}^T \begin{pmatrix} n_1\underline{\underline{\widetilde{\mathbf{S}}}}_{iso} & \underline{\underline{\mathbf{0}}} \\ \underline{\underline{\mathbf{0}}} & n_2\underline{\underline{\widetilde{\mathbf{S}}}}_{\mathbf{iso}} \end{pmatrix} \widetilde{\mathbf{Q}} = \frac{3}{5}\langle R^4\rangle q^4(n_1+n_2). \tag{A.6}$$

In summary, the signal for an isotropic orientation distribution of the cells and $q_1 = q_2 = q$ is

$$\begin{aligned} M_{\mathrm{iso}}(n_1,n_2,q,\theta) \propto\ & 1 - \frac{1}{3}(n_1+n_2)\langle R^2\rangle q^2 + \frac{1}{20}(n_1+n_2)\langle R^4\rangle q^4 \\ & + \left[\frac{1}{30}\left(n_1^2+n_2^2+n_1n_2-\frac{1}{2}(n_1+n_2)\right)\langle R_{kk}^2\rangle\right]q^4 \\ & + \left[\frac{n_1n_2}{30}\langle R_{kk}R_{ll}\rangle + \frac{n_1n_2}{30}\left(\langle R_{kk}^2\rangle - \langle R_{kk}R_{ll}\rangle\right)\cos 2\theta\right]q^4 \end{aligned} \tag{A.7}$$

or, for $n_1 = n_2 = n$,

$$\begin{aligned} M_{\mathrm{iso}}(n,q,\theta) \propto\ & 1 - \frac{2}{3}n\langle R^2\rangle q^2 \\ & + \left[\frac{1}{10}n\langle R^4\rangle + \frac{n^2}{10}\langle R_{kk}^2\rangle - \frac{n}{30}\langle R_{kk}^2\rangle\right]q^4 \\ & + \left[\frac{n^2}{30}\langle R_{kk}^2\rangle + \frac{n^2}{30}\left(\langle R_{kk}^2\rangle - \langle R_{kk}R_{ll}\rangle\right)\cos 2\theta\right]q^4. \end{aligned} \tag{A.8}$$

The microscopic anisotropy MA then yields the common expression

$$MA = \sqrt{\frac{1}{5}\langle R_{kk}^2\rangle - \frac{1}{5}\langle R_{kk}R_{ll}\rangle + \frac{3}{5}\langle R_{kl}^2\rangle}\Big/\langle R^2\rangle \tag{A.9}$$

which is identical to the value obtained for the case without concatenations [16].

In the θ-independent fourth order term of Eq. (A.9), $\langle R^4\rangle$ only appears with a prefactor of n while $\langle R_{kk}^2\rangle$ has terms proportional to n and n^2. This means for instance, that upon an variation of the number of concatenations n at constant q, $\langle R_{kk}^2\rangle$ can be determined from the fourth order signal contributions quadratic in n which in turn allows to calculate $\langle R^4\rangle$ from those linear in n.

References

[1] D.G. Cory, A.N. Garroway, J.B. Miller, Applications of spin transport as a probe of local geometry, Polym. Prepr. 31 (1990) 149–150.
[2] P.T. Callaghan, B. Manz, Velocity exchange spectroscopy, J. Magn. Reson. A 106 (1994) 260–265.
[3] P.P. Mitra, Multiple wave-vector extensions of the NMR pulsed-field-gradient spin-echo diffusion measurement, Phys. Rev. B 51 (1995) 15074–15078.
[4] P.T. Callaghan, D. MacGowan, K.J. Packer, F.O. Zelayam, High-resolution q-space imaging in porous structures, J. Magn. Reson. 90 (1990) 177–182.
[5] E.O. Stejskal, J.E. Tanner, Spin diffusion measurements: spin echoes in the presence of a time-dependent field gradient, J. Chem. Phys. 42 (1965) 288–292.

[6] M.A. Koch, J. Finsterbusch, Compartment size estimation with double wave vector diffusion-weighted imaging, Magn. Reson. Med. 60 (2008) 90–101.
[7] Y. Cheng, D.G. Cory, Multiple scattering by NMR, J. Am. Chem. Soc. 121 (1999) 7935–7936.
[8] M.A. Koch, J. Finsterbusch, Double wave vector diffusion weighting in the human corticospinal tract in vivo, in: Proceedings Int. Soc. Magn. Reson. Med., 16th Annual Meeting, Toronto, Canada, 2008, p. 764.
[9] T. Weber, C.H. Ziener, T. Kampf, V. Herold, W.R. Bauer, P.M. Jakob, Measurement of apparent cell radii using a multiple wave vector diffusion experiment, Magn. Reson. Med. 61 (2009) 1001–1006.
[10] M.A. Koch, J. Finsterbusch, In vivo pore size estimation in white matter with double wave vector diffusion weighting, in: Proceedings Int. Soc. Magn. Reson. Med., 18th Annual Meeting, Stockholm, Schweden, 2010, p. 194.
[11] Y. Qiao, P. Galvosas, P.T. Callaghan, Diffusion correlation NMR spectroscopic study of anisotropic diffusion of water in plant tissues, Biophys. J. 89 (2005) 2899–2905.
[12] P.T. Callaghan, M.E. Komlosh, Locally anisotropic motion in a macroscopically isotropic system: displacement correlations measured using double pulsed gradient spin-echo NMR, Magn. Reson. Chem. 40 (2002) S15–S19.
[13] M.E. Komlosh, F. Horkay, R.Z. Freidlin, U. Nevo, Y. Assaf, P.J. Basser, Detection of microscopic anisotropy in gray matter and in a novel tissue phantom using double pulsed gradient spin echo MR, J. Magn. Reson. 189 (2007) 38–45.
[14] M.E. Komlosh, M.J. Lizak, F. Horkay, R.Z. Freidlin, P.J. Basser, Observation of microscopic diffusion anisotropy in the spinal cord using double-pulsed gradient spin echo MRI, Magn. Reson. Med. 59 (2008) 803–809.
[15] M. Lawrenz, M.A. Koch, J. Finsterbusch, Evidence for microscopic diffusion anisotropy in spinal cord tissue observed with DWV imaging on a whole-body MR system, in: Proceedings Int. Soc. Magn. Reson. Med., 18th Annual Meeting, Stockholm, Schweden, 2010, p. 4005.
[16] M. Lawrenz, M.A. Koch, J. Finsterbusch, A tensor model and measures of microscopic anisotropy for double-wave-vector diffusion-weighting experiments with long mixing times, J. Magn. Reson. 202 (2010) 43–56.
[17] E. Özarslan, P.J. Basser, Microscopic anisotropy revealed by NMR double pulsed field gradient experiments with arbitrary timing parameters, J. Chem. Phys. 128 (2008) 154511-1–154511-11.
[18] E. Özarslan, Compartment shape anisotropy (CSA) revealed by double pulsed gradient field MR, J. Magn. Reson. 199 (2009) 56–67.
[19] M.A. Koch, J. Finsterbusch, Numerical simulation of double wave vector experiments investigating diffusion in randomly oriented ellipsoidal pores, Magn. Reson. Med. 62 (2009) 247–254.
[20] J. Finsterbusch, Extension of the double-wave-vector diffusion-weighting experiment to multiple concatenations, J. Magn. Reson. 198 (2009) 174–182.
[21] B.A. Auld, Acoustic Fields and Waves in Solids, vol. I, Wiley Interscience, New York, 1973.
[22] J. Finsterbusch, M.A. Koch, A tensor approach to double wave vector diffusion-weighting experiments on restricted diffusion, Magn. Reson. Med. 195 (2008) 23–32.
[23] D.C. Alexander, P.L. Hubbard, M.G. Hall, E.A. Moore, M. Ptito, G.J. Parker, and T.B. Dyrby, Orientationally invariant axon-size and density weighted MRI, in: Proceedings, Int. Soc. Magn. Reson. Med., 17th Annual Meeting, Hawaii, USA, 2009, p. 356.
[24] C.J. Rose, D. Ellard, D. Morris, H. Haroon, K. Embleton, N.K. Logothetis, M.A. Lambon Ralph, and G.J. Parker, A web-based probabilistic tractography database, in: Proceedings, Int. Soc. Magn. Reson. Med., 17th Annual Meeting, Hawaii, USA, 2009, p. 3552.
[25] R. Kimmlingen, E. Eberlein, M. Gebhardt, B. Hartinger, R. Ladebeck, R. Lazar, T. Reese, J. Riegler, F. Schmitt, G.A. Sorensen, V. Wedeen, L.L. Wald, An easy to exchange high performance head gradient insert for a 3T whole body MRI system: first results, in: Proceedings, Int. Soc. Magn. Reson. Med., 12th Annual Meeting, Kyoto, Japan, 2004, p. 1630.
[26] E. Özarslan, N. Shemesh, P.J. Basser, A general framework to quantify the effect of restricted diffusion on the NMR signal with applications to double pulsed field gradient NMR experiments, J. Chem. Phys. 130 (2009) 104702.